


ORIGINAL ARTICLE

Flow cytometric analysis of extracellular vesicle subsets in plasma: impact of swarm by particles of non-interest

S. F. W. M. LIBREGTS,*  G. J. A. ARKESTEIJN,* A. NÉMETH,† E. N. M. NOLTE-'T HOEN* and M. H. M. WAUBEN*

*Department of Biochemistry & Cell Biology, Faculty of Veterinary Medicine, Utrecht University, Utrecht, the Netherlands; and †Department of Genetics, Cell- and Immunobiology, Faculty of Medicine, Semmelweis University, Budapest, Hungary

To cite this article: Libregts SFWM, Arkesteijn GJA, Németh A, Nolte-'t Hoen ENM, Wauben MHM. Flow cytometric analysis of extracellular vesicle subsets in plasma: impact of swarm by particles of non-interest. *J Thromb Haemost* 2018; **16**: 1423–36.

Essentials

- Extracellular vesicles (EVs) in biological fluids are promising biomarkers for disease.
- Fluorescence-based flow cytometric analysis is suitable to detect low abundant EV subsets.
- Particles of non-interest can induce false-positive light scatter and fluorescent signals.
- Interference of particles of non-interest can be monitored by analyzing serial dilutions.

Summary. *Background:* Extracellular vesicles (EVs) in plasma are increasingly being recognized as potential biomarkers. EV analysis for diagnostic purposes should be robust and should allow analysis of EV subsets with a wide range of abundance and in a large number of patient samples. Flow cytometry offers possibilities to meet these criteria, as it allows multiparameter analysis of individual EVs. However, analysis of plasma EVs is challenging, because of their size and heterogeneity, and the presence of other submicrometer-sized particles in plasma that could interfere with EV analysis. *Objectives:* To explore whether fluorescence-based flow cytometric analysis of EV subsets is suitable when the EVs of interest are present in low abundance in a background of non-labeled or differently labeled EVs and particles. *Methods:* Fluorescently labeled EVs of interest were spiked at different ratios in full plasma, purified plasma components, or (non-)fluorescent polystyrene beads, and subsequently analyzed by flow cytometry with fluorescence threshold

triggering. *Results:* We found that light scatter detection of low-abundance or rare EV subsets during fluorescence threshold triggering was severely affected by particles of non-interest, owing to coincidence and swarming. Importantly, we show that interfering particles labeled with different fluorophores induced false-positive fluorescent signals on the particles of interest. These unwanted effects could only be discerned and controlled by performing serial dilutions and analyzing light scatter and fluorescence parameters. *Conclusions:* We demonstrate how particles of non-interest in plasma can impact on the light scatter and fluorescence detection of low-abundance EVs of interest during fluorescence-based flow cytometric analysis, and provide a means to prevent erroneous data interpretation.

Keywords: biomarkers; cell-derived microparticles; exosomes; extracellular vesicles; flow cytometry.

Correspondence: Sten F. W. M. Libregts, Department of Biochemistry & Cell Biology, Faculty of Veterinary Sciences, Utrecht University, Yalelaan 2, 3584 CM, Utrecht, the Netherlands
Tel.: +31 30 253 4342
E-mail: S.F.W.M.Libregts@uu.nl

Received: 4 May 2017

Manuscript handled by: P. H. Reitsma

Final decision: P. H. Reitsma, 27 April 2018

Introduction

Extracellular vesicles (EVs) are membrane-enclosed submicrometer-sized particles that are released by cells and play a role in intercellular communication [1–3]. The lipid, protein and nucleic acid composition of EVs largely determines their mode of action in target cells via receptor–ligand interactions or by transfer of their cargo [1,2]. Both the incorporation of molecules into EVs and the release of EVs are regulated processes that are dependent on the type and physiological state of individual cells [1,2]. Hence, EV populations in body fluids are heterogeneous. As the molecular content and the presence of specific EV subsets could contain information regarding the presence of disease, disease state, or efficiency of medical intervention, the biomarker potential of EVs is a subject of intense investigation [4–9].

EVs have been isolated from a variety of body fluids, including blood plasma [2]. However, because of their

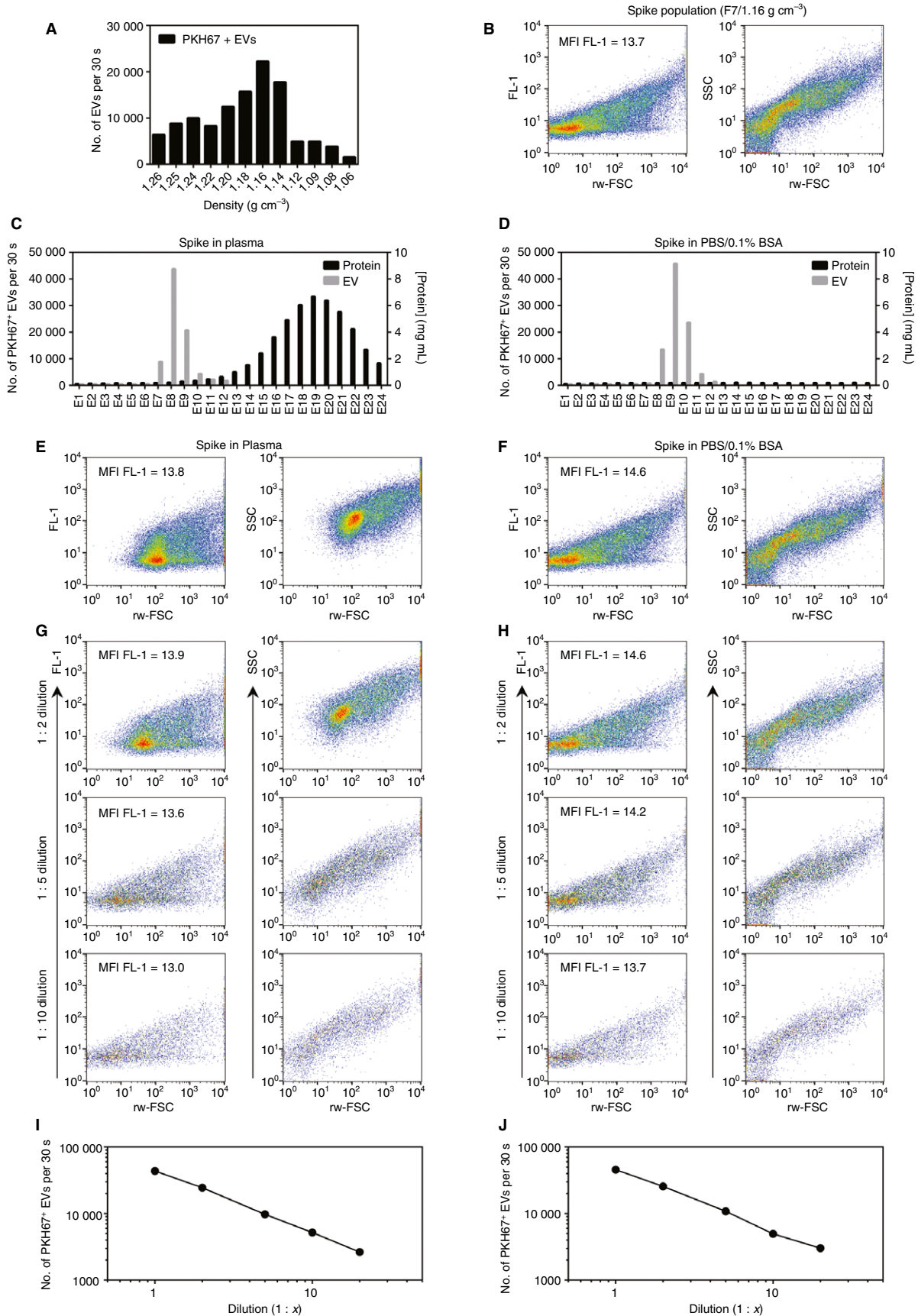


Fig. 1. Plasma-derived particles interfere with the light scatter detection of fluorescent extracellular vesicles (EVs) analyzed with fluorescence threshold triggering. A431 cells were cultured for 3 days in EV-depleted medium, after which EVs were isolated from the supernatant by differential centrifugation, stained with PKH67, and floated into a sucrose gradient. EV-containing sucrose fractions were diluted in phosphate-buffered saline (PBS) and analyzed with high-resolution flow cytometry. Fifty microliters of the sucrose fraction containing the highest concentration of EVs (F7) was then spiked into 450 μ L of plasma or PBS/0.1% bovine serum albumin (BSA). Spiked samples were subsequently eluted over qEV columns to separate EVs from plasma proteins and lipoprotein particles, and were analyzed for PKH67-positive EVs with high-resolution flow cytometry, and for proteins with photospectrometry. Serial dilutions of size-exclusion chromatography (SEC) eluates were prepared and analyzed. (A) Quantitative high-resolution flow cytometric analysis of EVs isolated from A431 cell culture supernatant. Bars show the PKH67-positive EV counts during a 30-s measurement in the various sucrose fractions diluted 1 : 40 in PBS. (B) Scatter plots showing FL-1 fluorescence, reduced wide-angle forward scatter (rw-FSC) and side scatter (SSC) of PKH67-positive EVs in sucrose fraction 7. (C, D) Bar graphs showing the recovery of PKH67-positive EVs and proteins in eluates obtained after performing SEC upon spiking PKH67-positive EVs in plasma or PBS/0.1% BSA. (E, F) Scatter plots of undiluted SEC eluates showing FL-1 fluorescence, rw-FSC and SSC of PKH67-positive EVs spiked in, respectively, plasma (eluate 8) or PBS/0.1% BSA (eluate 9). (G, H) Scatter plots showing FL-1 fluorescence, rw-FSC and SSC of PKH67-positive EVs in eluate 8 of the plasma-spiked sample or eluate 9 of the PBS/0.1% BSA-spiked sample upon serial dilution. (I, J) Analysis of the number of PKH67-positive EVs detected upon serial dilution of SEC eluates. All scatter plots represent a quantitative analysis of 30 s performed with fluorescence threshold triggering on the FL-1 channel. The experiment shown is representative of two independently performed experiments. MFI, mean fluorescence intensity. [Color figure can be viewed at wileyonlinelibrary.com]

submicrometer size, their heterogeneity, and the complexity of blood plasma, isolation and high-throughput analysis of individual EVs has proven to be a challenge [10,11]. Flow cytometry is often applied as a technique to gain insights into EV heterogeneity and the presence of EV subpopulations. However, considering that the vast majority of EVs are ≤ 500 nm in size, current commercially available flow cytometers are, in most cases, not designed for or capable of resolving individual EVs on the basis of light scatter [12–16]. Furthermore, blood plasma contains other submicrometer-sized particles (i.e. lipoproteins and protein complexes) that can be co-isolated and interfere with the detection of EVs [17–19]. Moreover, coincidence and swarming are processes that may occur during flow cytometric detection of small particles, and can lead to erroneous data interpretation. Coincidence in flow cytometry has been defined as occurring when two or more cells pass the measuring spot simultaneously, but can be distinguished [20,21], whereas swarming occurs when the concentration of particles in a sample is so high that light scatter or fluorescent signals generated by individual events can no longer be separated from each other, or when the concentration of submicrometer-sized particles is so high that their combined scatter or fluorescence value exceeds the detection limit and is detected as an event [22–24].

Most flow cytometers are more capable of resolving individual submicrometer-sized particles on the basis of fluorescent light, as fluorescence is less affected by background noise, thereby allowing better resolution of dim signals [21,25,26]. We and others have previously demonstrated the possibilities of fluorescence-based flow cytometric analysis of EVs [24–34]. By adapting a commercially available cell sorter and applying a generic strategy of fluorescent labeling of EVs in combination with antibody staining, we developed a high-resolution flow cytometric approach that allows quantitative and qualitative analysis of individual EVs and sorting of EV subsets [24–26]. The method entails an elaborate sample preparation procedure to efficiently eliminate confounding variables such as

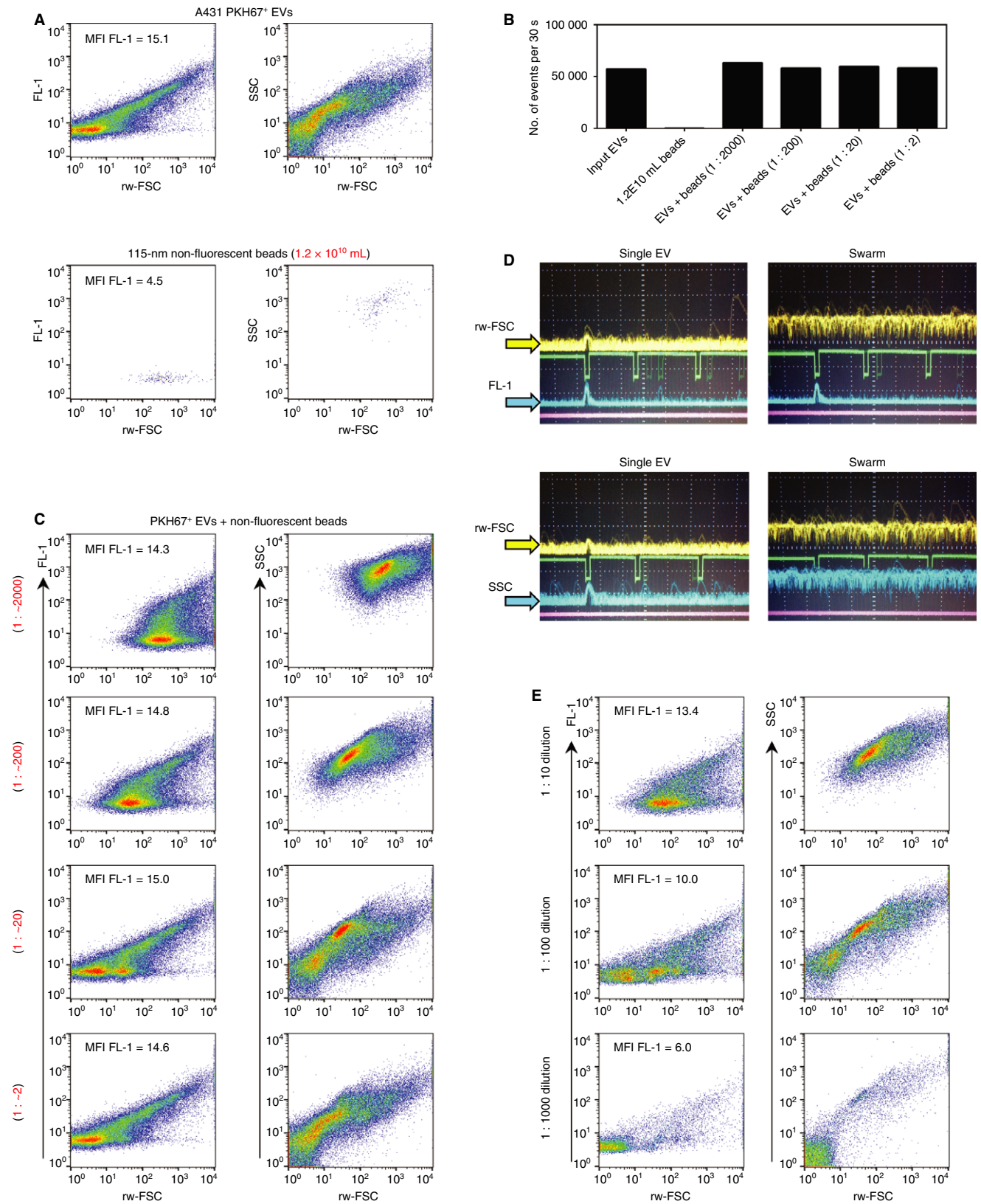
unincorporated dye, unbound fluorophore-conjugated antibodies, protein aggregates and other submicrometer-sized particles that can interfere with flow cytometric EV measurements [25,26]. Although it is useful in the discovery phase for biomarkers, this technically specialized procedure is labor-intensive and not well suited for high-throughput screening of samples. For clinical application of EV flow cytometry, sample preparation would ideally comprise minimal handling and processing. Size-exclusion chromatography (SEC) is currently widely applied as a simple EV isolation technique that efficiently enriches and separates the majority of EVs from proteins and subsets of lipoprotein particles in plasma [35,36]. As SEC also allows separation of EVs from unbound fluorophore-conjugated antibodies, it is a promising method with which to recover EVs from antibody-stained plasma samples prior to fluorescence-based flow cytometric analysis of EVs.

As disease-related EVs of interest in clinical samples are likely to be present in low abundance or as rare events, in the current study we determined the optimal conditions under which small subsets of fluorescently labeled EVs, spiked in plasma and purified by SEC, can be accurately quantified and characterized against a background of non-fluorescent or differently labeled submicrometer-sized particles by high-resolution flow cytometry.

Materials and methods

Isolation and staining of cell culture supernatant-derived EVs

For isolation of EVs from A431 (human epidermoid carcinoma) cell culture supernatants, 0.05% trypsin–EDTA (Gibco, Thermo Scientific, Waltham, MA, USA)-dissociated A431 cells were washed with L-glutamine-free Iscove's modified Dulbecco's medium (IMDM) (Life Technologies, Thermo Fisher Scientific, Bleiswijk, the Netherlands), resuspended at a concentration of 1.0×10^6 cells mL^{-1} in L-glutamine-free IMDM supplemented with 10% EV-depleted fetal bovine serum (FBS), 2 mM



ultraglutamine (BioWhittaker, Frederick, MD, USA), and 100 IU mL⁻¹ penicillin and streptomycin (Life Technologies, Thermo Fisher Scientific), and cultured in vented

T175 culture flasks (Corning, Amsterdam, the Netherlands) at 37 °C in 5% CO₂. EVs were removed from FBS by overnight centrifugation of 30% FBS in IMDM at 100 000 × g

Figure 2. Non-fluorescent bead swarms alter the light scatter detection of fluorescent extracellular vesicles (EVs) during fluorescence threshold triggering. A sucrose fraction containing PKH67-positive EVs isolated from A431 cell culture supernatant was diluted 1 : 20 in phosphate-buffered saline, spiked with various concentrations of non-fluorescent 115-nm polystyrene beads, and subsequently analyzed with high-resolution flow cytometry. Also, an EV sample spiked with a high concentration of beads (ratio 1 : 2000) was subjected to serial dilution and flow cytometric analysis. (A) Scatter plots showing FL-1 fluorescence, reduced wide-angle forward scatter (rw-FSC) and side scatter (SSC) of unspiked PKH67-positive EVs and the highest concentration of non-fluorescent 115-nm polystyrene beads (1.2×10^{10} mL). (B) Analysis of the rate of detected events upon spiking. (C) Scatter plots showing FL-1 fluorescence, rw-FSC and SSC of PKH67-positive EV samples spiked with different concentrations of non-fluorescent 115-nm polystyrene beads. The text in parentheses represents the PKH67-positive EV/non-fluorescent 115-nm polystyrene bead ratio. (D) Images of a digital oscilloscope showing baseline signals captured during measurement of an unspiked PKH67-positive EV sample (left: single EV measurement) and a PKH67-positive EV sample spiked with a high concentration of non-fluorescent 115-nm polystyrene beads (right: swarm). Yellow and blue arrows indicate the baseline signals of FL-1 fluorescence, rw-FSC, or SSC. (E) Scatter plots showing FL-1 fluorescence, rw-FSC and SSC upon serial dilution of a PKH67-positive EV sample that was spiked with non-fluorescent 115-nm polystyrene beads at a ratio of $\sim 1 : 2000$. Scatter plots represent a quantitative flow cytometric analysis of 30 s performed with fluorescence threshold triggering on the FL-1 channel. With the 1 : 10 and 1:100 dilutions, 30 000 events were acquired. With the 1 : 1000 dilution, 15 000 events were acquired. MFI, mean fluorescence intensity. [Color figure can be viewed at [wileyonlinelibrary.com](#)]

and 4 °C in polyallomer SW28 tubes (Beckman Coulter, Woerden, the Netherlands) by use of an SW28 or an SW32 rotor (Beckman Coulter). After overnight adherence, cells were washed with $1 \times$ phosphate-buffered saline (PBS) (Gibco, Thermo Scientific), and supplemented with fresh EV-depleted medium. After 3 days of culture, EVs were isolated from cell culture supernatant by differential centrifugation as described previously [26], but with minor modifications. Centrifugation steps of $10\,000 \times g$ and $100\,000 \times g$ were performed with an SW28 or an SW32 rotor, and $100\,000 \times g$ pellets were taken up in 20 μ L of PBS containing 0.1% aggregate-depleted bovine serum albumin (BSA). The BSA stock solution (5% [w/v] in PBS) was depleted of aggregates by overnight centrifugation at $100\,000 \times g$ and 4 °C in an SW28 or an SW32 rotor. Pelleted EVs were subsequently labeled with PKH67 (Sigma-Aldrich, St Louis, MO, USA), and separated from protein aggregates and free dye by overnight density gradient centrifugation at $270\,000 \times g$ with an SW40 rotor, according to the previously described protocol [26]. Gradient fractions were collected by pipetting 1-mL fractions from the top of the gradient. Densities of fractions were determined with refractometry, and the presence of EVs was analyzed with high-resolution flow cytometry. Samples were subsequently stored at 4 °C for further use in spiking experiments.

Preparation of platelet-free plasma (PFP)

Blood samples from healthy human donors were collected in sodium citrate at a final concentration of 3.2% (0.105 M), and processed within 1 h for optimal EV recovery. Samples were centrifuged at room temperature for 20 min at $2680 \times g$ with a tabletop centrifuge. Platelet-poor plasma was collected and spun for 5 min at room temperature and $10\,000 \times g$ with a tabletop centrifuge to deplete plasma samples of platelets. PFP samples were transferred to 1.5-mL tubes and stored at -80 °C. Collection of blood was approved by the ethics committees of the AMC Medical Center/University of Amsterdam. Participants provided written, informed consent.

Isolation of EVs by the use of SEC

For EV isolation from PFP, SEC columns (qEV; Izon Science, Oxford, UK) were used according to the manufacturer's protocol. Columns were calibrated and eluted with PBS/0.1% aggregate-depleted BSA. Eluates of 500 μ L were collected, and the protein content of eluted samples was determined by measuring absorbance at a wavelength of 280 nm with a NanoDrop 2000 UV-visible spectrophotometer (Thermo Scientific, Waltham, MA, USA).

High-resolution flow cytometric analysis of submicrometer-sized particles

High-resolution flow cytometric analysis of EV-containing samples was performed with a BD Influx (BD Biosciences, San Jose, CA, USA) that was modified and optimized for detection of submicrometer-sized particles [25,26] or with a CytoFLEX LX (Beckman Coulter). Detailed descriptions of modifications and methods are provided in Data S1.

Beads

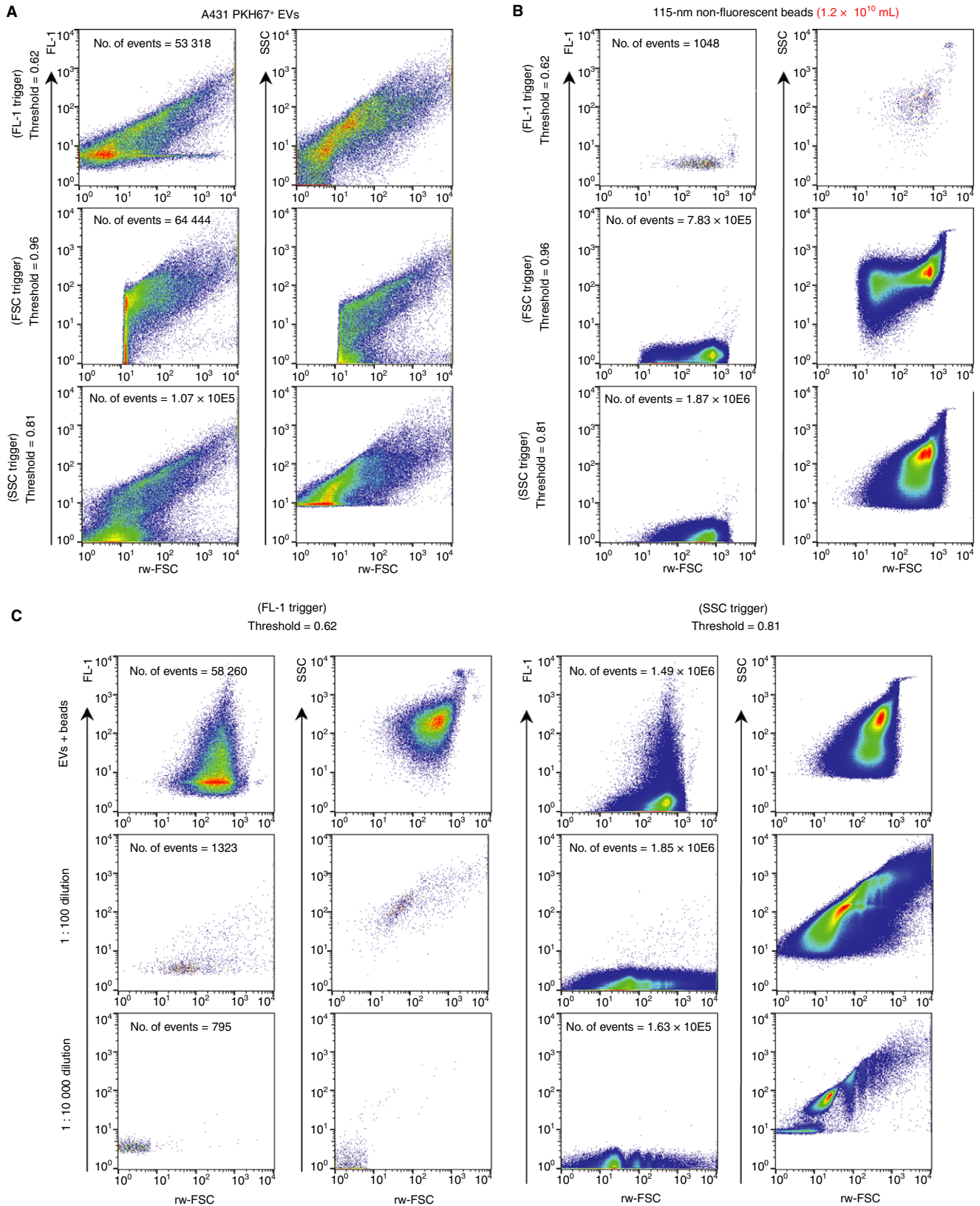
Fluorescent bead spike experiments were performed with 100-nm and 200-nm yellow-green (505/515) and 100-nm red (580/605) fluorescent carboxylate-modified polystyrene Fluosphere beads (Life Technologies, Thermo Fisher Scientific). Bead concentrations were calculated on the basis of the manufacturer's specifications. For spiking experiments with non-fluorescent beads, carboxylated polystyrene 115-nm qNano calibration particles (Izon Science) were used. Non-fluorescent bead concentrations were based on the manufacturer's specifications.

Western blot analysis

Two hundred and fifty microliters of qEV eluates 7–8–9 and 19–20–21 were transferred to polyallomer SW40 tubes (Beckman Coulter), topped up with PBS/0.1% aggregate-depleted BSA, and subjected to ultracentrifugation for 65 min at $270\,000 \times g$ and 4 °C in an SW40 rotor

(Beckman Coulter). Pellets were resuspended in non-reducing SDS-PAGE sample buffer, separated on a 12.5% SDS-PAGE gel, and transferred to a poly(vinylidene

difluoride) membrane (Millipore, Amsterdam-Zuidoost, the Netherlands). Membranes were blocked with PBS containing 5% (w/v) non-fat dry milk powder (Protifar Plus;



Nutricia, Zoetermeer, the Netherlands) and 0.1% Tween-20, and subsequently immunolabeled overnight with mouse anti-human CD9 (Biolegend, San Diego, CA, USA; clone HI9a, 1 : 1000) or mouse anti-human CD63 (BD Biosciences; clone H5C6, 1 : 500). Goat anti-mouse IgG+IgM (H+L) antibodies conjugated to horseradish peroxidase (Jackson ImmunoResearch, Ely, Cambridgeshire, UK; 1 : 10 000) were used as secondary antibodies, and detected with Supersignal West Dura Extended Duration chemiluminescent substrate (Thermo Fisher Scientific, Waltham, MA, USA). Imaging was performed with a Chemi-Doc MP system, and visualization was performed with IMAGE LAB v5.1 (Bio-Rad, Hercules, CA, USA).

Results

Plasma-derived particles interfere in the light scatter detection of fluorescent EVs analyzed with fluorescence threshold triggering

We investigated whether fluorescence-based flow cytometry allows accurate detection of a small subset of EVs of interest in plasma samples processed by SEC. For this purpose, we spiked fluorescently labeled EVs into unstained plasma, concurrently recovered both stained and unstained EVs by using SEC, and analyzed samples by using high-resolution flow cytometry (Fig. 1). EVs used for spiking were obtained by differential centrifugation of A431 cell culture supernatant, followed by labeling with PKH67 and subsequent purification by density-gradient centrifugation. PKH67-labeled EVs were efficiently detected with high-resolution flow cytometry by performing fluorescence threshold triggering on the FL-1 channel (PKH67) (Fig. 1A,B). The presence of EVs was further confirmed by analyzing CD9, tissue factor and epidermal growth factor receptor expression by flow cytometry (Fig. S1). Subsequently, PKH67-positive EVs were spiked into plasma or a PBS/0.1% BSA control sample, and eluted over SEC columns to separate EVs from contaminants such as proteins and lipoprotein particles. There was a clear separation of EVs from the bulk of plasma proteins (Fig. 1C,D), and the recovery of

PKH67-positive EVs from plasma was comparable to that of PKH67-positive EVs spiked in PBS/0.1% BSA, as indicated by the number of events obtained within a 30-s flow cytometric measurement (Fig. 1C,D). Strikingly, however, the light scatter parameters (side scatter [SSC] and reduced wide-angle forward scatter [rw-FSC]) of plasma-recovered PKH67-positive EVs were altered as compared with either PBS/0.1% BSA-recovered PKH67-positive EVs (Fig. 1E,F) or the initial starting population of PKH67-positive EVs (Fig. 1B). In contrast, the mean fluorescence intensity of detected EVs did not change (Fig. 1E,F). These data indicate that, when fluorescence threshold triggering is applied to detect an EV subset of interest in plasma, co-isolated plasma-derived particles can compromise light scatter-based analysis of these EVs.

EV samples that are measured in swarms show altered scatter patterns and a non-linear correlation between the event rate and EV concentration upon dilution [24]. We previously showed, on our flow cytometer, that, at event rates up to 10 000 events s^{-1} , no significant swarm effects occurred in sucrose gradient-purified PKH67-positive EV preparations [24]. Although the event rates of plasma-spiked PKH67-positive EVs were below the swarm-event rate and were fully comparable to the event rate of PKH67-positive EVs spiked in PBS/0.1% BSA (Fig. 1C, D), the light scatter patterns of plasma-spiked PKH67-positive EVs closely resembled those from EV samples measured with swarm interference [24]. In addition, no apparent alterations in height versus width plots could be observed (Fig. S2). To investigate whether swarm effects caused the interference in light scatter detection of the EVs of interest, we performed serial dilutions of the spiked samples. Interestingly, whereas the light scatter plots of PKH67-positive EVs spiked in PBS/0.1% BSA maintained their non-swarm characteristics throughout the dilution series (Fig. 1H), the light scatter plots of plasma-spiked PKH67-positive EVs changed upon dilution (Fig. 1G), and, at high dilution, resembled the light scattering of the initial starting population of PKH67-positive EVs (Fig. 1B). Remarkably, however, the event rate showed a linear correlation with the PKH67-positive EV concentration upon serial dilution, both when EVs

Fig. 3. Non-fluorescent bead swarms during fluorescence threshold triggering can be detected by switching to light scatter detection. A sucrose fraction containing PKH67-positive extracellular vesicles (EVs) isolated from A431 cell culture supernatant was diluted 1 : 20 in 1 mL of phosphate-buffered saline (PBS), spiked with a high concentration of non-fluorescent 115-nm polystyrene beads, and subsequently analyzed with high-resolution flow cytometry with either fluorescence threshold triggering or light scatter-based detection. (A) Scatter plots showing FL-1 fluorescence, reduced wide-angle forward scatter (rw-FSC) and side scatter (SSC) of unspiked PKH67-positive EVs upon fluorescence (FL-1 trigger)-based, forward scattered light (FSC trigger)-based and sideward scattered light (SSC trigger)-based detection. (B) Scatter plots showing FL-1 fluorescence, rw-FSC and SSC of 1.2×10^{10} mL non-fluorescent 115-nm polystyrene beads in PBS upon an FL-1 trigger, an FSC trigger, and an SSC trigger. (C) Scatter plots showing FL-1 fluorescence, rw-FSC and SSC of a dilution range of a 1-mL PKH67-positive EV sample spiked with 1.2×10^{10} mL non-fluorescent 115-nm polystyrene beads. Detection of events was performed with fluorescence threshold triggering (FL-1 trigger) or triggering on sideward scattered light (SSC trigger). Scatter plots represent a quantitative flow cytometric analysis of 30 s; numbers within the plots represent the number of events detected during the measurement. The threshold for detection was determined by acquiring a PBS control sample and allowing approximately 20 background events per second during fluorescence threshold triggering and 100–150 events per second during light scatter triggering. The experiment shown is representative of two independently performed experiments. [Color figure can be viewed at wileyonlinelibrary.com]

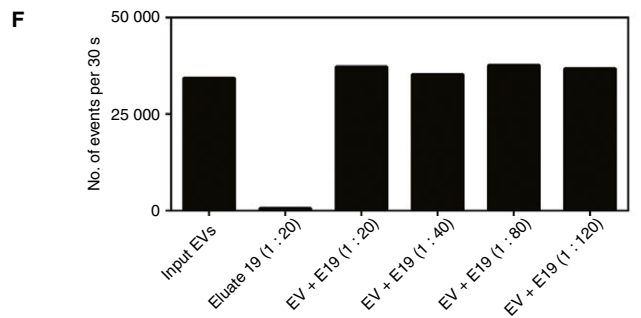
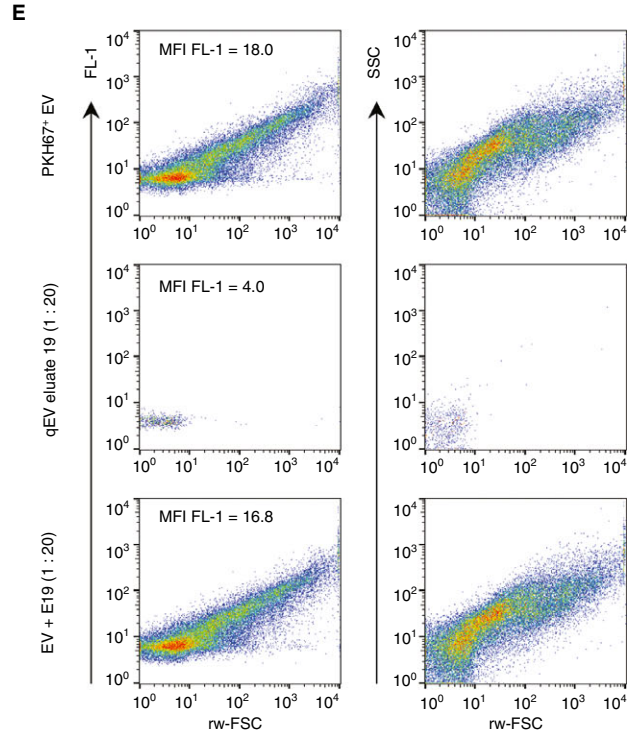
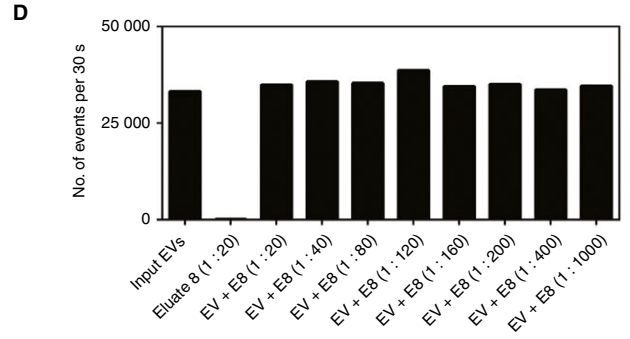
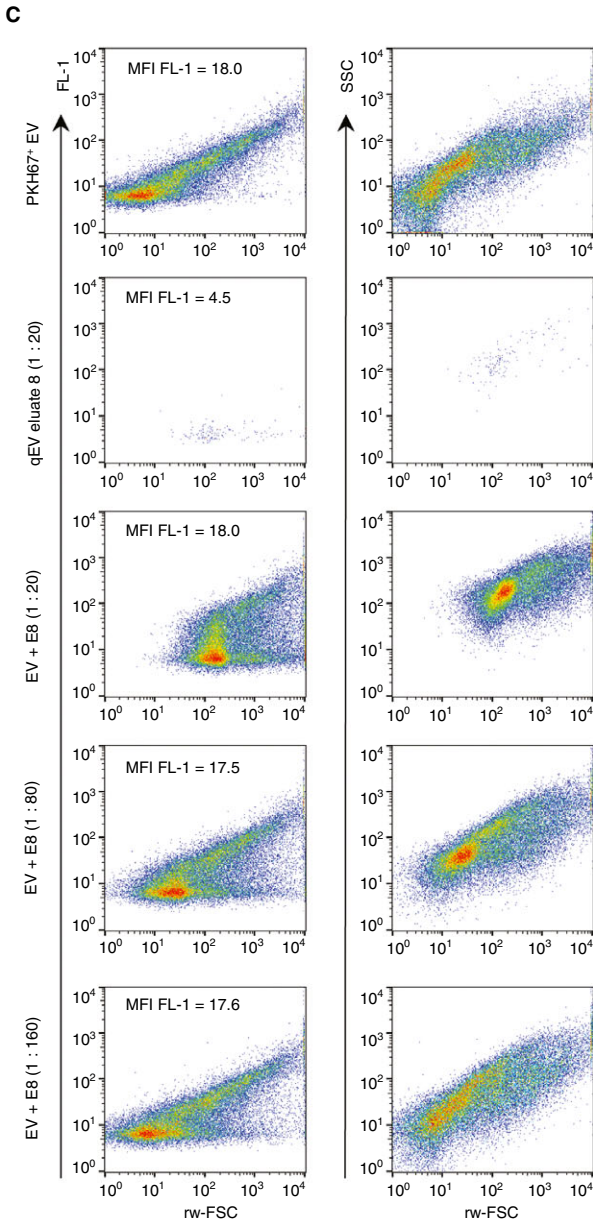
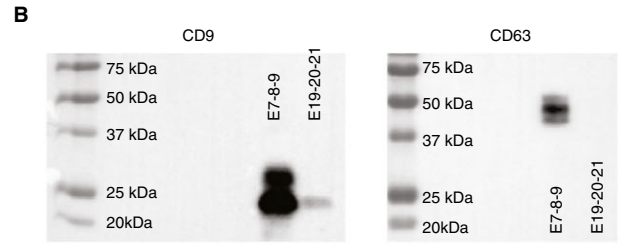
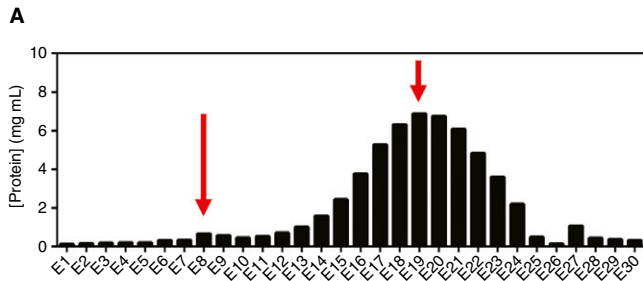


Fig. 4. Extracellular vesicle (EV)-containing size-exclusion chromatography (SEC) fractions of plasma affect the light scatter of fluorescent EVs of interest during fluorescence threshold triggering. One milliliter of unstained plasma was eluted over an SEC column to separate EVs from proteins and HDL. Eluates were analyzed for the presence of EVs with western blotting, and for the presence of proteins with photospectrometry. Different concentrations of EV-containing eluate 8 and protein-containing eluate 19 were spiked in PKH67-positive EV-containing samples (sucrose fraction diluted 1 : 20 in phosphate-buffered saline). PKH67-positive EVs were isolated from the cell culture supernatant of A431 cells by differential centrifugation, stained with PKH67, floated into a sucrose gradient, and analyzed with high-resolution flow cytometry. (A) Protein content analysis of SEC eluates from plasma. (B) Western blot analysis for CD9 and CD63 on a pool of SEC eluates (7–8–9 and 19–20–21) from plasma. (C) Scatter plots showing FL-1 fluorescence, reduced wide-angle forward scatter (rw-FSC) and side scatter (SSC) of a PKH67-positive EV sample, an SEC eluate 8 sample diluted 1 : 20, and PKH67-positive EV samples spiked with different concentrations of SEC eluate 8. (D) Analysis of the rate of detected fluorescent events upon spiking of PKH67-positive EVs with SEC eluate 8 samples. (E) Scatter plots showing FL-1 fluorescence, rw-FSC and SSC of a PKH67-positive EV sample, an SEC eluate 19 sample at a dilution of 1 : 20, and a PKH67-positive EV sample spiked with SEC eluate 19 at a dilution of 1 : 20. (F) Analysis of the rate of detected events upon spiking of PKH67-positive EVs in SEC eluate 19 samples. Scatter plots represent a quantitative flow cytometric analysis of 30 s performed with fluorescence threshold triggering on the FL-1 channel. The experiment shown is representative of two independently performed experiments. MFI, mean fluorescence intensity. [Color figure can be viewed at wileyonlinelibrary.com]

were spiked in plasma and when they were spiked in PBS/0.1% BSA (Fig. 1I,J). This suggests that the altered light scatter patterns were not caused by a swarm of the fluorescent EVs, but rather by swarms of non-fluorescent particles that were co-isolated from plasma by SEC. As these phenomena were also observed when fluorescently labeled EVs were spiked in breast milk (Fig. S3), these data collectively suggest that, when fluorescence threshold triggering is applied to detect a small subset of EVs within biological fluids, high concentrations of co-isolated non-fluorescent particles can induce swarming and affect light scatter detection of fluorescent EVs of interest.

Non-fluorescent bead swarms alter light scatter detection of fluorescent EVs during fluorescence threshold triggering

To directly investigate the influence of non-fluorescent submicrometer-sized particles on light scatter detection of a fluorescent EV subpopulation of interest, we spiked different concentrations of non-fluorescent 115-nm polystyrene beads in samples containing a fixed number of PKH67-positive EVs. Whereas the PKH67-positive EVs could easily be detected by threshold triggering on the FL-1 signal, the highest concentrations of non-fluorescent beads ($1.2 \times 10^{10} \text{ mL}^{-1}$) were not detectable (Fig. 2A), and showed a similar event count as a PBS control sample (data not shown). When the PKH67-positive EV sample was spiked with non-fluorescent beads at a ratio of 1 : 2000, the event rate of detected EVs remained unaltered (Fig. 2B), whereas the light scatter patterns were severely affected (Fig. 2C). This was accompanied by a distortion of the signal pulses for SSC and rw-FSC, but not FL-1 fluorescence, as observed on the oscilloscope attached to the flow cytometer (Fig. 2D). Although single fluorescent EVs induced a clear signal pulse for SSC, rw-FSC, and FL-1, a swarm of non-fluorescent particles in the sample hampered the baseline restoration function for SSC and rw-FSC, resulting in a general increase in signal (Fig. 2D). When lower concentrations of non-fluorescent beads were added to PKH67-positive EV-containing samples (Fig. 2C), or when the PKH67-positive EV sample

spiked with a high concentration of non-fluorescent beads was diluted (Fig. 2E), the light scatter patterns altered, and finally resembled the light scatter plots of the starting population of PKH67-positive EVs (Fig. 2A). In addition, SSC and rw-FSC signals on the oscilloscope normalized (data not shown). Similar results were obtained when non-fluorescent beads were spiked in 100-nm yellow-green Fluosphere bead-containing samples (Fig. S4). Hence, these data collectively show that high numbers of non-fluorescent submicrometer-sized particles can induce swarming and affect the light scatter of fluorescently labeled EVs detected by fluorescence threshold triggering. Because, under these circumstances, the event rate is not indicative of the presence of a swarm, induction of a swarm by particles of non-interest can only be detected after serial dilution of the sample and subsequent monitoring of light scatter and fluorescent parameters in scatter plots and accompanying pulse shapes on a digital oscilloscope. Alternatively, interference by particles of non-interest during fluorescence threshold triggering can be exposed by switching from fluorescence threshold triggering to light scatter-based detection. Although the light scatter signals of smaller EVs are obscured by background noise (Fig. 3A, indicated by the increase in the threshold for detection) and detection is less sensitive than with fluorescence threshold triggering (Fig. 3A), it does allow identification of non-fluorescent particle swarms that are otherwise not detected by fluorescence-threshold triggering (Fig. 3B,C). Determining a proper dilution of the sample, followed by switching back to fluorescence-based detection, is, however, troublesome, as smaller events will be present underneath the detection threshold.

EV-containing SEC fractions of plasma affect the light scatter of fluorescent EVs of interest during fluorescence threshold triggering

Next, we investigated which non-fluorescent particles in plasma can affect the detection of fluorescently labeled EVs during fluorescence threshold triggering. We

performed SEC on unstained plasma to separate EVs from proteins, HDL, and other small particles (Fig. 4A) [35]. To verify the presence of plasma-derived EVs, pools of SEC eluates 7–8–9 (E7–8–9) and 19–20–21 (E19–20–21) were prepared, pelleted, and analyzed for the presence of CD9 and CD63 by western blotting. E7–8–9 contained both CD9 and CD63, which is indicative of the presence of EVs (Fig. 4B). In E19–20–21, a weak signal for CD9 was found, whereas CD63 was absent, suggesting that, besides the presence of proteins and HDL, a low number of, most likely, small EVs were present in this fraction (Fig. 4B). E8, containing EVs, and E19, containing proteins and smaller particles, were subsequently spiked into a fixed number of PKH67-positive EVs. No specific events were detected in dilutions of the E8 and E19 fractions with fluorescence-based triggering (Fig. 4C,E). As in the previous observations, the event rate and the fluorescence intensity of detected PKH67-positive EVs remained unaltered after spiking with E8 (Fig. 4C,D), whereas the light scatter plots showed a concomitant alteration in SSC and rw-FSC (Fig. 4C). This did not occur after spiking with E19 (Fig. 4E,F). When E8 was further diluted upon spiking (Fig. 4C), or when the PKH67-positive EV sample spiked with highly concentrated E8 was serially diluted (Fig. S5), scatter plots changed, and finally resembled that of the original PKH67-positive EV sample. These data show that, upon fluorescence threshold triggering, high concentrations of non-fluorescent EVs from plasma can affect the light scattering analysis of EVs of interest by induction of swarming.

Beads of non-interest carrying a fluorescent label can generate false-positive fluorescence on beads of interest

Because, for multiparameter analysis of single EVs and EV subset analysis, samples need to be stained with antibodies conjugated to different fluorophores, we next evaluated whether background particles labeled with a different fluorescent marker can affect fluorescent signals of particles of interest. To test such potential interference effects, we performed a proof-of-principle experiment by using different fluorescently labeled beads. We spiked different concentrations of 100-nm red fluorescent Fluosphere beads (red beads, representing the interfering particles) into a fixed number of 100-nm yellow–green Fluosphere beads (green beads, representing the particles of interest), and performed fluorescence threshold triggering to detect the green beads (FL-1). Whereas the green beads could be clearly visualized above the threshold (Fig. 5A, first row), the red beads, which cannot be excited by the trigger laser, were not detected, and showed an event rate comparable to that of a PBS background measurement (Fig. 5A, second row). When a high concentration of red beads was subsequently spiked in a sample containing green beads (green/red ratio of $\sim 1 : 100$), the event rate of detected green beads was not

affected (Fig. 5B); however, the light scatter parameters changed, and, more importantly, red-positive events (FL-3) were now observed (Fig. 5A, third row). The red fluorescence could not have been generated by the green beads, but instead was derived from red beads that, owing to their high concentration, co-localized with the green beads in the measuring spot. Indeed, when the concentration of red beads was lowered (Fig. 5A), or when samples containing green beads and a high concentration of red beads ($\sim 1 : 100$) were diluted, the signal for red fluorescence disappeared (Fig. 5A,C). As expected, serial dilution of the green beads spiked with red beads resulted in a linear decrease in the measured events (Fig. 5D). In reciprocal experiments, where red bead-containing samples were spiked with high concentrations of green beads, altered light scatter parameters and false-positive green events were observed when fluorescence threshold triggering was performed on the fluorescence derived from the red beads (Fig. S6). This phenomenon is not cytometer-specific, as comparable results were obtained on a flow cytometer with sufficient resolution for fluorescence-based submicrometer-sized particle detection and digital signal processing (Figs S7 and S8). Together, these data thus show that, when fluorescence threshold triggering is performed on a sample in which a subset of fluorescently labeled submicrometer-sized particles is present among high numbers of differently labeled submicrometer-sized particles, swarm detection of the latter particles not only affects light scatter detection of particles of interest, but can also generate false-positive fluorescent signals.

Discussion

In this study, we identified factors that affect the flow cytometric analysis of fluorescently labeled subpopulations of EVs in plasma. We show that, when fluorescence threshold triggering is performed on biological samples in which the fluorescent EVs of interest constitute only a small percentage of the total EV population, the detection of these EVs can be heavily obscured by high concentrations of EVs and other submicrometer-sized particles that lack the fluorescent label needed for detection. When these EVs or particles are present within the measuring spot upon detection of a fluorescent EV of interest, they are not identified as individual events. Rather, the light scatter signals generated by this ‘invisible’ particle swarm are detected and falsely integrated and attributed to the EV of interest. More importantly, when the interfering particles are labeled with different fluorophores, they can induce false-positive fluorescent signals on the particle of interest. Serial dilution of samples allows detection of particle swarms that interfere with the detection of the EVs of interest, as both light scatter and fluorescent signals alter until the point is reached when only single EVs or particles are present in the measuring spot. As the concentration of EVs and submicrometer-particles in general,

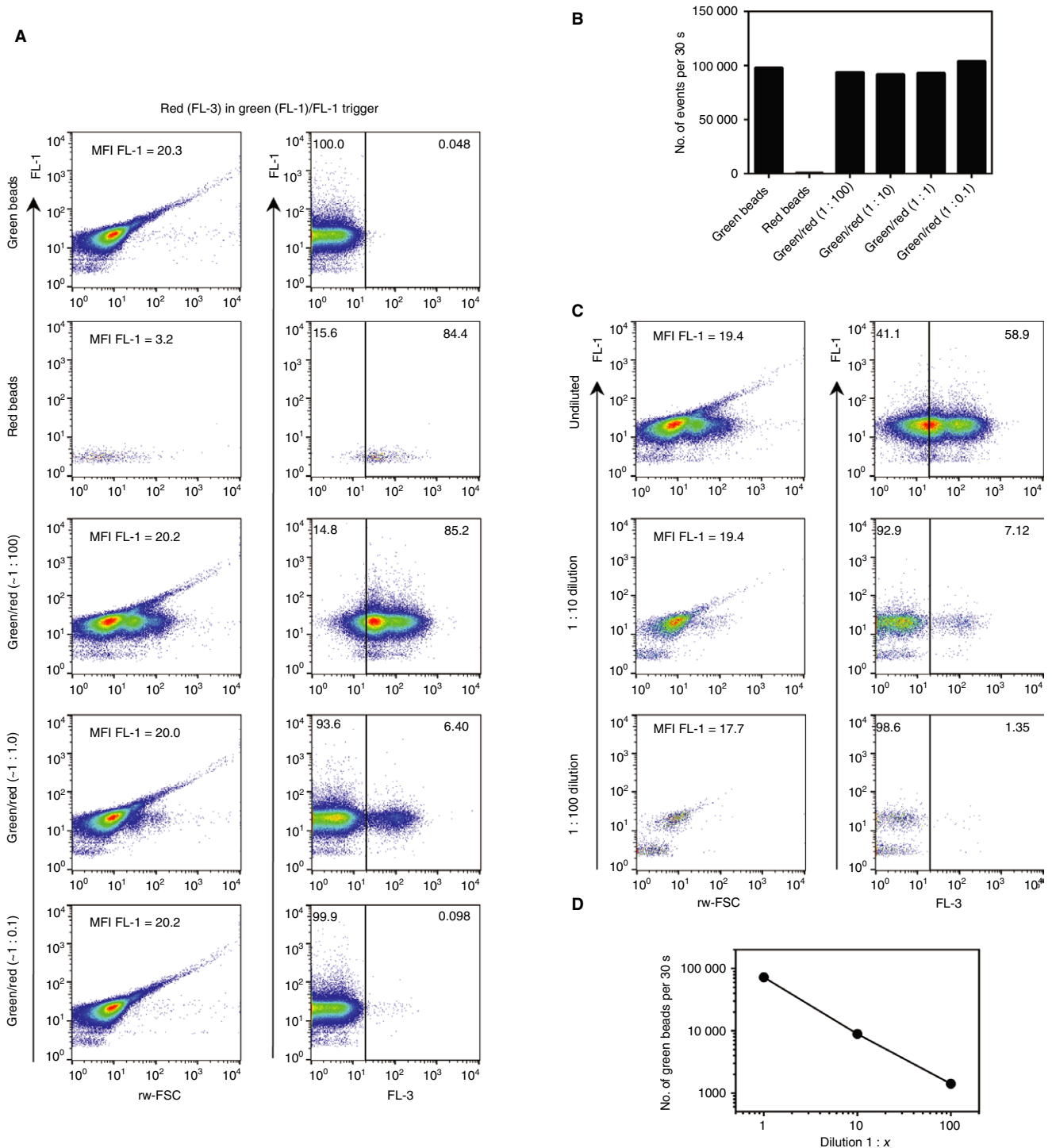


Fig. 5. Beads of non-interest carrying a fluorescent label can generate false-positive fluorescence on beads of interest. Fixed amounts of 100-nm yellow-green fluorescent (505/515) Fluosphere beads (green beads, FL-1) were spiked in different concentrations of 100-nm red fluorescent (580/605) Fluosphere beads (red beads, FL-3). Samples were subsequently analyzed with high-resolution flow cytometry. Also, a green bead sample spiked with a high concentration of red beads (1 : 100) was serially diluted and reanalyzed. (A) Scatter plots showing FL-1 fluorescence, reduced wide-angle forward scatter (rw-FSC), side scatter (SSC) and FL-3 fluorescence of green beads, the highest concentration of red beads, and green beads spiked with different concentrations of red beads. (B) Analysis of the rate of detected events upon spiking different concentration of red beads into a fixed number of green beads. (C) Scatter plots showing FL-1 fluorescence, rw-FSC, SSC and FL-3 fluorescence of green beads spiked with a high concentration of red beads (1 : 100), followed by serial dilution. (D) Analysis of the event rate of a spiked sample upon serial dilution. Scatter plots represent a quantitative analysis of 30 s performed with fluorescence threshold triggering on the FL-1 channel. The experiment shown is representative of two independently performed experiments. MFI, mean fluorescence intensity. [Color figure can be viewed at wileyonlinelibrary.com]

and the percentage of fluorescently labeled EVs of interest in particular, are mostly unknown and variable in biological samples, to exclude swarm interference application of serial dilutions and subsequent monitoring of light scatter and fluorescent parameters is recommended when a fluorescence-based detection strategy is used. Depending on the concentrations of the EVs of interest and interfering particles within a sample, the event rate may drop significantly, while the acquisition time increases substantially.

Although invisible particle swarms can qualitatively affect the light scatter and fluorescent signals of EVs of interest during fluorescence threshold triggering, they have no or only very limited impact on the quantitative measurements. This is illustrated by the fact that, upon spiking of different concentrations of non-fluorescent EVs or submicrometer-sized particles into a fixed number of fluorescently labeled EVs, the trigger signal was unchanged and the event rate remained unaffected. The event rate is therefore not a good indicator of the presence of 'invisible' particle swarms during fluorescence-based detection of EV subsets. This is further substantiated by the fact that, upon serial dilution of a sample affected by an invisible swarm, the light scatter and fluorescent parameters of events of interest varied, whereas there was a linear correlation between the event rate and the dilution factor.

To further control the impact of invisible particles during fluorescence threshold triggering on EV subsets, electronic signal pulses can be monitored. If a digital oscilloscope is attached to the flow cytometer, signal pulses of light scatter and fluorescence parameters can be visualized during measurements [24]. During fluorescence threshold triggering, the pulse for the fluorescent trigger signal remains unaffected in the presence of interference by events of non-interest, whereas pulses for other parameters are distorted. In this case, samples should be diluted to a point at which the pulses of forward scatter, SSC and fluorescence channels remain constant at further dilution. Alternatively, 'invisible' swarm interference can be revealed by switching to light scatter-based detection. Although this allows the detection of non-fluorescent particles that remained unidentified upon fluorescence threshold triggering, determination of a proper sample dilution is hampered by the lower sensitivity of scatter-based triggering.

We show that the 'invisible' swarm phenomenon appeared on two different flow cytometers with resolution for fluorescence-based submicrometer-sized particle detection. Because of differences in optics, fluidics, and signal pulse-processing architecture, measurements on different flow cytometers might be more or less affected by interference by submicrometer-sized particles during fluorescence-based detection of EVs. Nonetheless, the ratio between EVs of interest and interfering EVs or particles of non-interest plays an important role in whether sample analysis can be affected by particle swarms. Previously,

fluorescence threshold triggering on EV subsets in plasma and ascites was successfully performed [30,32,33]. With the use of fluorophore-conjugated antibodies, EV subsets were detected in these biological fluids, and by performance of serial dilutions the presence of coincidence and swarming was excluded [32,33]. However, in these studies the EV subsets of interest constituted a significant proportion of the total EV pool, and measurements were therefore less prone to interference by non-fluorescently or differently labeled EVs and particles. Our data substantiate the finding that fluorescence threshold triggering allows for the accurate detection of abundant EV subsets; however, we show that, when the percentage of EVs of interest decreases in the total EV population, the chance of swarming and thereby erroneous data interpretation increases. This is especially important when fluorescent threshold triggering is applied in clinical settings, where EVs of interest are likely to be present in low abundance or as rare events.

In conclusion, our findings urge cautious use of the fluorescence-based threshold triggering approach to analyze EV subpopulations that are likely to constitute only a small percentage of the EV or submicrometer-sized particle population within the sample. The performance of serial dilutions and the use of an oscilloscope to monitor pulse shapes is strongly recommended to control for erroneous swarm effects.

Addendum

S. F. W. M. Libregts designed research, performed experiments, analyzed data, and wrote the manuscript. G. J. A. Arkesteijn designed research, analyzed data, and reviewed the manuscript. A. Németh performed experiments, analyzed data, and reviewed the manuscript. E. N. M. Nolte-*t* Hoen designed research, analyzed data, and reviewed the manuscript. M. H. M. Wauben designed research, analyzed data, and reviewed the manuscript.

Acknowledgements

This research was supported by the Dutch Technology Foundation STW (Perspectief Program Cancer ID, project 14191), which is part of the Netherlands Organization for Scientific Research (NWO), and which is partly funded by the Ministry of Economic Affairs. The authors would like to thank R. Nieuwland and A. Böing for kindly providing PFP samples, and F. Salerno for critical reading of the manuscript.

Disclosure of Conflict of Interests

During this study, the Wauben research group, Utrecht University, Faculty of Veterinary Medicine, Department of Biochemistry and Cell Biology had a collaborative research agreement with BD Biosciences Europe,

Erembodegem, Belgium, to optimize analysis of EVs with the BD Influx. S. F. W. M. Libregts reports receiving grants from the Dutch Technology Foundation STW (Perspectief Program Cancer ID, project 14191), a part of the Netherlands Organization for Scientific Research (NWO), which is partly funded by the Ministry of Economic Affairs, during the conduct of the study. The other authors state that they have no conflict of interest.

Supporting Information

Additional supporting information may be found online in the Supporting Information section at the end of the article.

Data S1. Supplementary methods.

Table S1. Laser, PMT and filter setup for high-resolution flow cytometric analysis of EVs and submicrometer-sized particles.

Fig. S1. Characterization of A431-derived extracellular vesicles.

Fig. S2. Impossibility of performing doublet exclusion during flow cytometric analysis of EVs.

Fig. S3. Milk-derived particles interfere with light scatter detection of fluorescent EVs analyzed using fluorescence threshold triggering.

Fig. S4. Non-fluorescent bead swarm alters light scattering of fluorescent beads during fluorescence threshold triggering.

Fig. S5. EV-containing SEC fractions of plasma affect light scatter of fluorescent EVs of interest during fluorescence threshold triggering.

Fig. S6. Beads of non-interest carrying a fluorescent label can generate false-positive fluorescence on beads of interest.

Fig. S7. Beads of non-interest carrying a fluorescent label can generate false-positive fluorescence on beads of interest.

Fig. S8. Beads of non-interest carrying a fluorescent label can generate false-positive fluorescence on beads of interest.

Fig. S9. High-resolution flow cytometry setup of BD Influx using polystyrene Fluosphere beads.

Fig. S10. Flow cytometry setup of CytoFLEX LX using polystyrene Fluosphere beads.

References

- Théry C, Ostrowski M, Segura E. Membrane vesicles as conveyors of immune responses. *Nat Rev Immunol* 2009; **9**: 581–93.
- Yáñez-Mó M, Siljander PR-M, Andreu Z, Zavec AB, Borràs FE, Buzas EI, Buzas K, Casal E, Cappello F, Carvalho J, Colás E, Cordeiro-da Silva A, Fais S, Falcon-Perez JM, Ghebrial IM, Giebel B, Gimona M, Graner M, Gursel I, Gursel M, *et al.* Biological properties of extracellular vesicles and their physiological functions. *J Extracell Vesicles* 2015; **4**: 27066.
- Tkach M, Théry C. Communication by extracellular vesicles: where we are and where we need to go. *Cell* 2016; **164**: 1226–32.
- György B, Szabó TG, Pászti M, Pál Z, Misják P, Aradi B, László V, Pállinger E, Pap E, Kittel A, Nagy G, Falus A, Buzás EI. Membrane vesicles, current state-of-the-art: emerging role of extracellular vesicles. *Cell Mol Life Sci* 2011; **68**: 2667–88.
- van der Pol E, Böing AN, Harrison P, Sturk A, Nieuwland R. Classification, functions, and clinical relevance of extracellular vesicles. *Pharmacol Rev* 2012; **64**: 676–705.
- El Andaloussi S, Mäger I, Breakefield XO, Wood MJA. Extracellular vesicles: biology and emerging therapeutic opportunities. *Nat Rev Drug Discov* 2013; **12**: 347–57.
- Cheng L, Sharples RA, Scicluna BJ, Hill AF. Exosomes provide a protective and enriched source of miRNA for biomarker profiling compared to intracellular and cell-free blood. *J Extracell Vesicles* 2014; **3**: 1–14.
- Revenfeld ALS, Bæk R, Nielsen MH, Stensballe A, Varming K, Jørgensen M. Diagnostic and prognostic potential of extracellular vesicles in peripheral blood. *Clin Ther* 2014; **36**: 830–46.
- Julich H, Willms A, Lukacs-Kornek V, Kornek M. Extracellular vesicle profiling and their use as potential disease specific biomarker. *Front Immunol* 2014; **5**: 413.
- Witwer KW, Buzás EI, Bemis LT, Bora A, Lässer C, Lötvall J, Nolte-’t Hoen EN, Piper MG, Sivaraman S, Skog J, Théry C, Wauben MH, Hochberg F. Standardization of sample collection, isolation and analysis methods in extracellular vesicle research. *J Extracell Vesicles* 2013; **2**: 1–25.
- Xu R, Greening DW, Zhu H-J, Takahashi N, Simpson RJ. Extracellular vesicle isolation and characterization: toward clinical application. *J Clin Invest* 2016; **126**: 1152–62.
- Lacroix R, Robert S, Poncelet P, Kasthuri RS, Key NS, Dignat-George F. Standardization of platelet-derived microparticle enumeration by flow cytometry with calibrated beads: results of the International Society on Thrombosis and Haemostasis SSC Collaborative workshop. *J Thromb Haemost* 2010; **8**: 2571–4.
- Chandler WL, Yeung W, Tait JF. A new microparticle size calibration standard for use in measuring smaller microparticles using a new flow cytometer. *J Thromb Haemost* 2011; **9**: 1216–24.
- Robert S, Poncelet P, Lacroix R, Raoult D, Dignat-George F. More on: calibration for the measurement of microparticles: value of calibrated polystyrene beads for flow cytometry-based sizing of biological microparticles. *J Thromb Haemost* 2011; **9**: 1676–8.
- Mullier F, Bailly N, Chatelain C, Dogné JM, Chatelain B. More on: Calibration for the measurement of microparticles: needs, interests, and limitations of calibrated polystyrene beads for flow cytometry-based quantification of biological microparticles. *J Thromb Haemost* 2011; **9**: 1679–81.
- Cointe S, Judicone C, Robert S, Mooberry MJ, Poncelet P, Wauben M, Nieuwland R, Key NS, Dignat-George F, Lacroix R. Standardization of microparticle enumeration across different flow cytometry platforms: results of a multicenter collaborative workshop. *J Thromb Haemost* 2016; **15**: 1–7.
- György B, Módos K, Pállinger É, Pálóczi K, Pászti M, Misják P, Deli MA, Sipos Á, Szalai A, Voszka I, Polgár A, Tóth K, Csete M, Nagy G, Gay S, Falus A, Kittel Á, Buzás EI. Detection and isolation of cell-derived microparticles are compromised by protein complexes resulting from shared biophysical parameters. *Blood* 2011; **117**: 39–49.
- Yuana Y, Levels J, Grootemaat A, Sturk A, Nieuwland R. Co-isolation of extracellular vesicles and high-density lipoproteins using density gradient ultracentrifugation. *J Extracell Vesicles* 2014; **3**: 1–5.
- Sódar BW, Kittel Á, Pálóczi K, Vukman KV, Osteikoetxea X, Szabó-Taylor K, Németh A, Sperlágh B, Baranyai T, Giricz Z, Wiener Z, Turiák L, Drahos L, Pállinger É, Vékey K, Ferdinandy P, Falus A, Buzás EI. Low-density lipoprotein mimics blood plasma-derived exosomes and microvesicles during isolation and detection. *Sci Rep* 2016; **6**: 24316.
- Shapiro HM. *Practical Flow Cytometry*. 4th edn. New York, NY: Wiley-Liss, 2003.

- 21 Nolan JP. Flow cytometry of extracellular vesicles: potential, pitfalls, and prospects. *Curr Protoc Cytom* 2015; **2015**: 13.14.1–16.
- 22 Van Der Pol E, Van Gemert MJC, Sturk A, Nieuwland R, Van Leeuwen TG. Single vs. swarm detection of microparticles and exosomes by flow cytometry. *J Thromb Haemost* 2012; **10**: 919–30.
- 23 Nolan JP, Stoner SA. A trigger channel threshold artifact in nanoparticle analysis. *Cytom Part A* 2013; **83**: 301–5.
- 24 Kormelink TG, Arkesteijn GJA, Nauwelaers FA, van den Engh G, Nolte-t Hoen ENM, Wauben MHM. Prerequisites for the analysis and sorting of extracellular vesicle subpopulations by high-resolution flow cytometry. *Cytom Part A* 2016; **89**: 135–47.
- 25 Hoen t ENMN, van der Vlist EJ, Aalberts M, Mertens HCH, Bosch BJ, Bartelink W, Mastrobattista E, van Gaal EVB, Stoorvogel W, Arkesteijn GJA, Wauben MHM. Quantitative and qualitative flow cytometric analysis of nanosized cell-derived membrane vesicles. *Nanomed Nanotechnol* 2012; **8**: 712–20.
- 26 van der Vlist EJ, Nolte-t Hoen ENM, Stoorvogel W, Arkesteijn GJA, Wauben MHM. Fluorescent labeling of nano-sized vesicles released by cells and subsequent quantitative and qualitative analysis by high-resolution flow cytometry. *Nat Protoc* 2012; **7**: 1311–26.
- 27 van der Vlist EJ, Arkesteijn GJA, van de Lest CHA, Stoorvogel W, Nolte-t Hoen ENM, Wauben MHM. T cell activation promotes the differential release of distinct populations of nanosized vesicles. *J Extracell Vesicles* 2012; **1**: 1–9.
- 28 Nolte-t Hoen ENM, van der Vlist EJ, de Boer-Brouwer M, Arkesteijn GJA, Stoorvogel W, Wauben MHM. Dynamics of dendritic cell-derived vesicles: high-resolution flow cytometric analysis of extracellular vesicle quantity and quality. *J Leukoc Biol* 2013; **93**: 395–402.
- 29 Erdbrügger U, Rudy CKE, Etter M, Dryden KA, Yeager M, Klibanov AL, Lannigan J. Imaging flow cytometry elucidates limitations of microparticle analysis by conventional flow cytometry. *Cytom Part A* 2014; **85**: 756–70.
- 30 Arraud N, Gounou C, Linares R, Brisson AR. A simple flow cytometry method improves the detection of phosphatidylserine-exposing extracellular vesicles. *J Thromb Haemost* 2015; **13**: 237–47.
- 31 Stoner SA, Duggan E, Condello D, Guerrero A, Turk JR, Narayanan PK, Nolan JP. High sensitivity flow cytometry of membrane vesicles. *Cytom Part A* 2016; **89**: 196–206.
- 32 Pospichalova V, Svoboda J, Dave Z, Kotrbova A, Kaiser K, Klemova D, Ilkovic L, Hampl A, Crha I, Jandakova E, Minar L, Weinberger V, Bryja V. Simplified protocol for flow cytometry analysis of fluorescently labeled exosomes and microvesicles using dedicated flow cytometer. *J Extracell Vesicles* 2015; **4**: 25530.
- 33 Arraud N, Gounou C, Turpin D, Brisson AR. Fluorescence triggering: a general strategy for enumerating and phenotyping extracellular vesicles by flow cytometry. *Cytom Part A* 2016; **89**: 184–95.
- 34 Morales-Kastresana A, Telford B, Musich TA, McKinnon K, Clayborne C, Braig Z, Rosner A, Demberg T, Watson DC, Karpova TS, Freeman GJ, DeKruyff RH, Pavlakis GN, Terabe M, Robert-Guroff M, Berzofsky JA, Jones JC. Labeling extracellular vesicles for nanoscale flow cytometry. *Sci Rep* 2017; **7**: 1878.
- 35 Böing AN, Van Der Pol E, Grootemaat AE, Coumans FA, Sturk A, Nieuwland R. Single-step isolation of extracellular vesicles from plasma by size-exclusion chromatography. *Int Meet ISEV Rotterdam* 2014; **3**: 118.
- 36 Lobb RJ, Becker M, Wen SW, Wong CSF, Wiegman AP, Leimgruber A, Möller A. Optimized exosome isolation protocol for cell culture supernatant and human plasma. *J Extracell Vesicles* 2015; **1**: 1–11.